Nearly Room-Temperature Ferromagnetism in a Pressure-Induced Correlated Metallic State of the van der Waals Insulator $CrGeTe_3$

Dilip Bhoi,[1,*] Jun Gouchi,[1] Naoka Hiraoka,[2] Yufeng Zhang,[1,3] Norio Ogita,[4] Takumi Hasegawa,[4] Kentaro Kitagawa,[2] Hidenori Takagi,[2,5,6] Kee Hoon Kim,[7,8] and Yoshiya Uwatoko[1]

[1]*The Institute for Solid State Physics, University of Tokyo, Kashiwa, Chiba 277-8581, Japan*
[2]*Department of Physics, Graduate School of Sciences, University of Tokyo, Tokyo 113-0033, Japan*
[3]*School of Physics, Southeast University, Nanjing 211189, China*
[4]*Graduate School of Integrated Arts and Sciences, Hiroshima University, Higashi-Hiroshima, Hiroshima 739-8521, Japan*
[5]*Institute for Functional Matter and Quantum Technologies, University of Stuttgart, 70569 Stuttgart, Germany*
[6]*Max Planck Institute for Solid State Research, Heisenbergstraße 1, 70569 Stuttgart, Germany*
[7]*Department of Physics and Astronomy, CeNSCMR, Seoul National University, Seoul 151-747, Republic of Korea*
[8]*Institute of Applied Physics, Seoul National University, Seoul 151-747, Republic of Korea*

(Received 12 July 2021; accepted 8 October 2021; published 17 November 2021)

A complex interplay of different energy scales involving Coulomb repulsion, spin-orbit coupling, and Hund's coupling energy in 2D van der Waals (vdW) material produces a novel emerging physical state. For instance, ferromagnetism in vdW charge transfer insulator $CrGeTe_3$ provides a promising platform to simultaneously manipulate the magnetic and electrical properties for potential device implementation using few nanometers thick materials. Here, we show a continuous tuning of magnetic and electrical properties of a $CrGeTe_3$ single crystal using pressure. With application of pressure, $CrGeTe_3$ transforms from a ferromagnetic insulator with Curie temperature $T_C \sim 66$ K at ambient condition to a correlated 2D Fermi metal with T_C exceeding ~250 K. Notably, absence of an accompanying structural distortion across the insulator-metal transition (IMT) suggests that the pressure induced modification of electronic ground states is driven by electronic correlation furnishing a rare example of bandwidth-controlled IMT in a vdW material.

DOI: 10.1103/PhysRevLett.127.217203

The discovery of 2D magnetism in van der Waals (vdW) materials has unfurled a diverse range of possibilities for development of novel spintronics, multiferroic and quantum computing devices using atomically thin material, as well as fundamental research [1–6]. These also include exploration of exotic physics such as Kitaev quantum spin liquid state in $3d$ electron system with $S = 3/2$ [7,8]. Until now, $CrYTe_3$ (Y = Ge, Si) [9,10], CrX_3 (X = I and Br) [11–15], 1T-$CrTe_2$ [16,17] and $Fe_{3-x}GeTe_2$ [18–21] have been the few vdW materials known to exhibit ferromagnetic (FM) order in bulk single crystal form and retain intrinsic ferromagnetism down to the monolayer limit. Among these, $CrYTe_3$ and CrX_3 are Mott insulators with a charge gap, facilitating a suitable platform to exploit both charge and spin degrees of freedom.

At low temperature, these Cr-based vdW insulators share a common layered rhombohedral $R\bar{3}$ crystal structure held together by weak vdW forces along the c axis [10–12]. Each single layer consists of a honeycomb network of edge sharing octahedra formed by a central Cr atom bonded to six ligand atoms (Te or X), as illustrated in Fig. 1(a) for $CrGeTe_3$ as a representative. Crystalline field effect ensuing from this octahedra splits Cr-3d orbitals into t_{2g} manifolds and e_g manifolds [Fig. 1(b)]. The onsite Coulomb repulsion localizes the t_{2g} electrons driving the system into an insulating state significantly well above the Curie temperature, T_C [22–24]. Although a direct antiferromagnetic (AFM) exchange interaction exists between t_{2g} electrons, thermal fluctuation inherent to 2D suppresses the long-range magnetic order. The spin-orbit coupling (SOC) emanating through the covalent bond between the ligand p and Cr-e_g orbital generates the magnetocrystalline anisotropy energy (MAE) to counteract the thermal fluctuation [24,25]. Below T_C, superexchange interaction between the active Cr-e_g electrons via two different ligand p orbitals, as schematically portrayed in Fig. 1(c), benefits from distortion of $CrTe_6$ octahedra and Hund's energy gain at the ligand Te (or X) site to stabilize the FM order [22,24,26]. Moreover, correlation between t_{2g} electrons moves up the ligand p bands close to the Fermi level, thus opening a band gap between the Cr d-conduction band and ligand p-valence band, confirming the charge transfer type Mott behavior [22–24,26,27].

The charge gap of a Mott insulator can be manipulated either by carrier doping which fills the band or by controlling the bandwidth, resulting in an insulator-metal transition (IMT) often accompanied by structural and magnetic transitions. So far, doping through gating a field effect transistor (FET) device [28–30], or intercalation of organic ions to bulk single crystals [31] have been used.

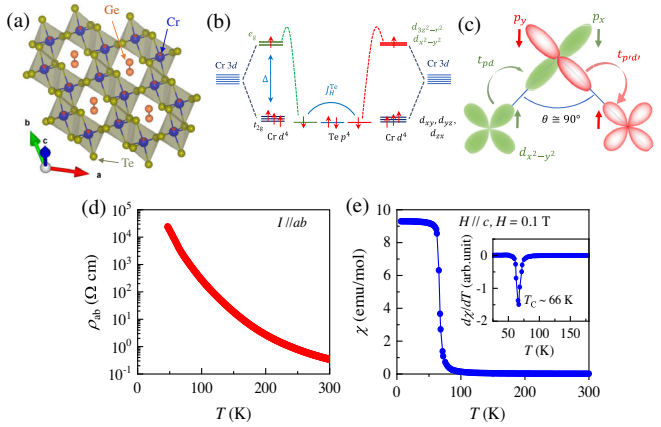

FIG. 1. (a) A single layer of $CrGeTe_3$. In CrX_3, the place of Ge-Ge dimers remains vacant. (b) Crystalline electric field splitting of Cr $3d$ orbitals into t_{2g} manifolds and e_g manifolds. Δ is the energy difference between t_{2g} levels and e_g levels. J_H^{Te} is the Hund's coupling energy at the Te site. (c) Schematic picture of FM superexchange interaction between Cr e_g orbitals via two Te p orbitals. $t_{pd}(t_{p'd'})$ is the virtual hopping between $e_g(e_g')$ and $p(p')$ orbitals. θ is the geometrical Cr—Te—Cr bond angle. (d) In plane resistivity, ρ_{ab}. (e) Zero field-cooled (ZFC) magnetic susceptibility χ at $H = 0.1$ T applied along c axis. Inset: temperature derivative of $d\chi/dT$.

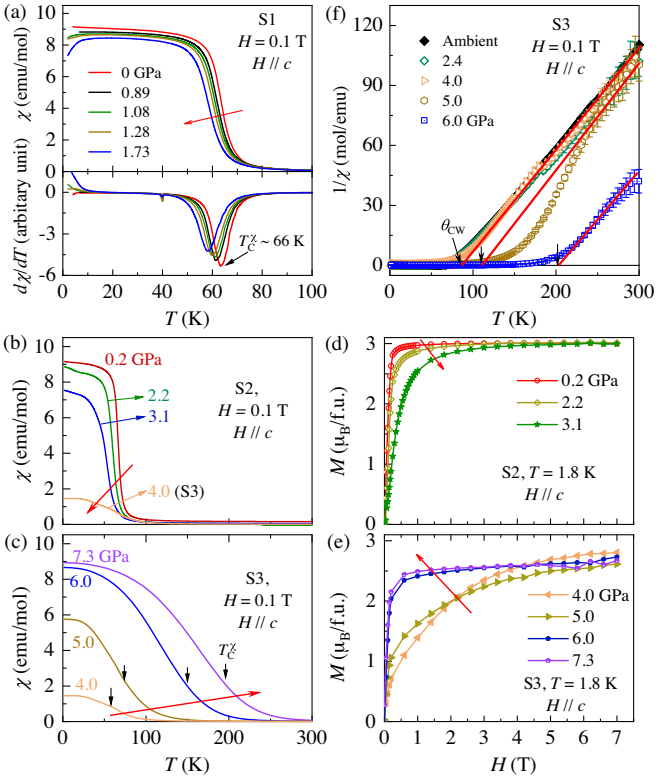

FIG. 2. (a) Top: ZFC dc susceptibility of $CrGeTe_3$ crystal $S1$ up to 1.73 GPa. Bottom: temperature dependence of $d\chi/dT$. Field-cooled (FC) susceptibility for crystal (b) $S2$ and (c) $S3$. Field dependence of magnetization, $M(H)$, for (d) $S2$ and (e) $S3$ at $T = 1.8$ K under different pressure. Red arrows represent the direction of increasing pressure. (f) Curie-Weiss plot, $1/\chi$ vs T, of crystal $S3$ at some selected pressure.

With electrostatic gating to few layers of $CrGeTe_3$ [28] and CrI_3 [29], the coercive field and saturation magnetization are found to be modulated, but T_C changes barely. However, when high carrier density ($\sim 10^{-14}$ cm^{-2}) is doped to $CrGeTe_3$ either through intercalation [31] or ionic liquid gating to FET devices [30], T_C around $\sim$200 K is achieved with simultaneous stabilization of a metallic state. Although these results are promising, nevertheless, such filling-controlled methods lead to undesirable effects such as strong charge inhomogeneity in atomic scale either due to disorder created by intercalant ions or chemical modification of the host material induced by ionic liquid [32].

On the contrary, application of pressure is an alternative route, which not only controls the bandwidth but also the spin exchange pathways via subtle modification of bond length and angle between atoms avoiding the complication of disorder. Pressure has been suitably used to switch the interlayer magnetism of few layers of CrI_3 [33,34] including the T_C variation of CrI_3 and $CrGeTe_3$ bulk single crystals [35–37]. However, these studies are limited to less than 2.0 GPa with T_C varying about $\sim$10%. Interestingly, a recent high pressure work on $CrSiTe_3$ [38] revealed a concomitant structural transition and IMT followed by a superconductivity around 7.0 GPa.

In this Letter, we study the electronic and magnetic properties of $CrGeTe_3$ single crystals by varying pressure up to 11.0 GPa using dc magnetic susceptibility and resistivity measurement. Although the pressure dependent lattice dynamics of $CrGeTe_3$ have been performed revealing a 2D to 3D structural transition around ≥ 18 GPa [35,39], the magnetic and electrical properties at high pressure have remain unexplored. At ambient pressure, $CrGeTe_3$ is an insulator with a band gap of $\sim$0.7 eV [40] and orders in a Heisenberg-type ferromagnetism below $T_C \sim 66$ K as shown in Figs. 1(d) and 1(e). At first, T_C decreases monotonically to 54 K when pressure increases to 4.5 GPa. Remarkably, T_C jumps fourfold in between $4.5 \leq P \leq 7.5$ GPa and surpasses 250 K above 9.1 GPa. In addition, the pressure temperature phase diagram uncovers an IMT to a correlated Fermi metallic state above $\sim$7.0 GPa, characterized by large resistivity anisotropy, $\rho_c/\rho_{ab} \sim 10^5$, suggesting a 2D nature of charge transport. Our results suggest that a collapse of the charge transfer energy gap between the Te p-valence band and Cr e_g-conduction band dramatically boosts the intralayer FM superexchange interaction producing such a high T_C.

In the top panel of Fig. 2(a), we illustrate the temperature dependence of dc susceptibility χ of $CrGeTe_3$ single crystal ($S1$) with an applied field $H = 0.1$ T parallel to the c axis at several pressures. At ambient pressure, $\chi(T)$ undergoes a typical paramagnet (PM) to FM transition, and the estimated $T_C^{\chi} \sim 66$ K, from the minimum of $d\chi/dT$ curve is

consistent with several earlier reports [40–42]. With increasing pressure up to 1.73 GPa [Fig. 2(a)], the transition shifts toward a lower temperature, and T_C^{χ} reduces to ~58 K at 1.73 GPa [bottom panel of Fig. 2(a)]. The weak downturn of χ below ~7.0 K at 1.08 GPa is related to the formation of FM domains in the crystal as evidenced by the bifurcation between FC and ZFC curve [see Fig. S2 in the Supplemental Material [43]]. To track further the evolution of T_C above 2.0 GPa, we measured χ of another two pieces of $CrGeTe_3$ single crystals extracted from the same batch using an opposed-anvil-type pressure cell [44]. Figures 2(b) and 2(c) present the temperature dependence of χ for crystals $S2$ and $S3$, respectively. Although the magnitude of χ decreases drastically as pressure is raised to 4.0 GPa [Fig. 2(b)], T_C^{χ} decreases modestly to ~54 K. Surprisingly, as pressure is increased further the magnitude of χ surges again and transition shifts toward a higher temperature [Fig. 2(c)]. For $P \cong 5.0$ GPa, $\chi(T)$ curves show a broad transition to a FM state with $T_C^{\chi} \sim 73$ K. At 7.3 GPa, T_C^{χ} reaches to ~196 K, almost 3 times higher than the T_C^{χ} at ambient pressure. The broad transition at high pressure could be due to the pressure inhomogeneity inside the sample space arising from the solidification of pressure transmitting media (for details, see Supplemental Material [43]).

In Figs. 2(d) and 2(e), we present the $M(H)$ curve along the easy magnetization c axis for crystals $S2$ and $S3$, respectively. At 0.2 GPa, the $M(H)$ curve saturates sharply at $H_S \cong 0.22$ T with a saturation moment $M_S \sim 3.0\ \mu_B$/f.u.. With variation of pressure the $M(H)$ curve becomes rounder and H_S surpasses 3.0 T at 3.1 GPa. At 4.0 GPa, the $M(H)$ curve looks similar to a Brillouin-like function and does not saturate even up to 7.0 T. Even though the $M(H)$ curve resembles to a PM, the Curie-Weiss temperature θ_{CW} at this pressure is comparable with that of ambient condition, hinting at the presence of strong FM interaction [see Fig. 2(f)]. For $P \geq 5.0$ GPa, H_S start to decrease again. At $P \cong 6.0$ GPa, the $M(H)$ curve saturates sharply above $H_S \simeq 0.18$ T with $M_S \sim 2.76\ \mu_B$/f.u., a typical sign of FM order. From the evolution of $\chi(T)$ and $M(H)$ curves under pressure, it is clear that in the intermediate pressure range $3.1\ \text{GPa} \leq P \leq 5.0$ GPa, the net FM exchange interaction weakens, producing a diminished $\chi(T)$ magnitude and T_C^{χ}.

Next, in Fig. 3(a) we show the temperature dependence of in plane resistivity ρ_{ab} of $CrGeTe_3$ under different pressure revealing an IMT. The overall ρ_{ab} plummet several orders of magnitude as 11.0 GPa pressure is applied; at low temperature ρ_{ab} falls more than 9 orders of magnitude, while at $T = 300$ K more than 3 orders. At 2.0 GPa, $\rho_{ab}(T)$ discloses a shoulderlike anomaly at $T_C^{\rho} \sim 59$ K, very close to the FM transition observed in $\chi(T)$, allowing one to trace the evolution of magnetic order with pressure from ρ_{ab} data. T_C^{ρ} falls to ~54 K at 4.5 GPa. However, at 5.0 GPa, ρ_{ab} exhibits a broad maximum at ~73 K [Fig. 3(b)], an indication of T_C^{ρ} moving to high temperature in agreement

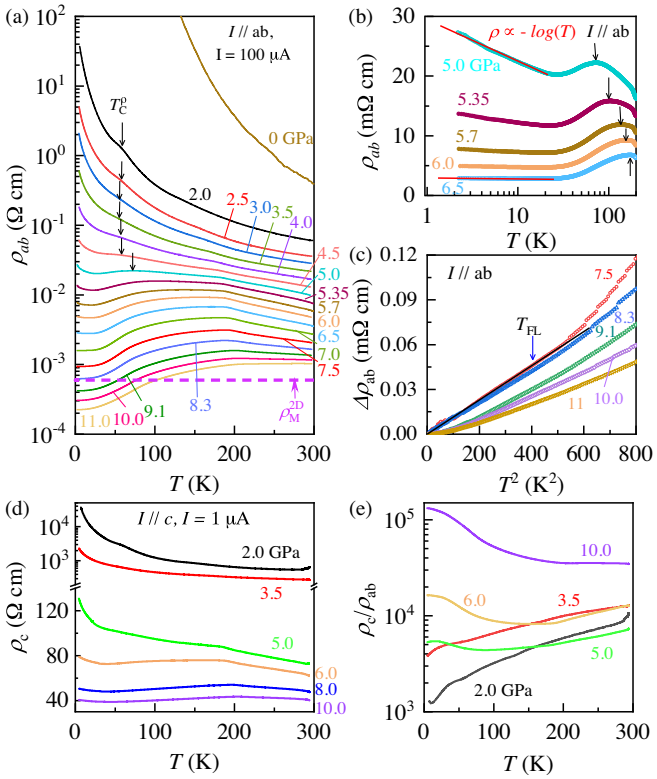

FIG. 3. (a) In plane resistivity ρ_{ab} of $CrGeTe_3$ at several pressures ranging from 0 to 11.0 GPa. The magenta dotted line represents an estimate of the Mott-Ioffe-Regel limit of resistivity, ρ_M^{2D}. (b) ρ_{ab} in logarithmic temperature scale. Red solid lines are $-\log(T)$ fit to ρ_{ab}. (c) $\Delta\rho_{ab} = (\rho_{ab} - \rho_0)$ vs T^2 for $P \geq 7.5$ GPa, where ρ_0 is the residual resistivity. The black line is a linear fit to $\Delta\rho_{ab}$ at 7.5 GPa confirming a Fermi liquid state below T_{FL}. (d) Out of plane resistivity ρ_c and (e) resistivity anisotropy ρ_c/ρ_{ab} at some selected pressure.

with the T_C^{χ} of $\chi(T)$. Additionally, ρ_{ab} reveals a weak upturn below ~25 K, where it follows a $-\log(T)$ dependence with decreasing temperature suggesting a 2D weak localization behavior. On compressing further to 7.0 GPa, T_C^{ρ} surges rapidly to 193 K consistent with $\chi(T)$ data. At the same time, the $-\log(T)$ upturn in ρ_{ab} is gradually suppressed uncovering a metallic state. At high pressure, precise determination of T_C^{ρ} becomes difficult due to the broad anomaly, yet signature of $T_C^{\rho} \sim 250$ K can be traced up to 9.1 GPa.

At 7.0 GPa, ρ_{ab} follows a power law, $\rho_{ab} = \rho_0 + AT^n$ with an exponent $n \sim 1.9$ below $T_{FL} \sim 14$ K, a hallmark of the Fermi-liquid (FL) state. It is worthy to note that at this pressure, ρ_{ab} is higher than the Mott-Ioffe-Regel limit of resistivity defined as $\rho_M^{2D} \cong 0.055(c/a_0) \sim 0.6$ mΩ cm, where c is the average separation between $CrGeTe_3$ layers and $a_0 = 0.529$ Å is the Bohr radius [52]. Besides, the residual resistivity ratio (RRR), $\rho_{300\,K}/\rho_{2\,K} \simeq 2$ clearly indicates a bad metal behavior. The RRR and temperature window, where $\rho_{ab} < \rho_M^{2D}$, increases with rising pressure. Simultaneously, T_{FL} grows to 56 K at 11.0 GPa [Fig. 3(c)],

and the A coefficient of the T^2 term drops by more than 2 orders of magnitude, a clear indication of a widening of the FL region at higher pressure with decreasing correlation strength.

To obtain more insight about this metallic state, we measured interlayer resistivity ρ_c of another piece of single crystal from the same batch as shown in Fig. 3(d). Unlike ρ_{ab}, ρ_c continue to be semiconducting down to the lowest temperature at 6.0 GPa. Intriguingly, ρ_c is nearly temperature independent deep inside the metallic state even at 10.0 GPa, conveying an incoherent interlayer charge transport and confinement of charge carriers in the ab plane. This becomes increasingly clear from the temperature dependence of resistivity anisotropy ρ_c/ρ_{ab} as in shown Fig. 3(e). For $P < 5.0$ GPa, $\rho_c/\rho_{ab} \simeq 10^3$–$10^4$, whereas ρ_c/ρ_{ab} reaches as high as $\sim 10^5$ at 10.0 GPa and 2 K. Such a large value of ρ_c/ρ_{ab} is comparable with that of several strongly correlated materials like high-T_c cuprates [53], manganites [54], and organic compounds [55]. Thus, the pressure-induced metallic state in $CrGeTe_3$ can be regarded as an ideal 2D correlated Fermi metal.

The P-T phase diagram [Fig. 4(a)], constructed from susceptibility and resistivity data, unveils a fascinating evolution of the electronic and magnetic properties of $CrGeTe_3$ when pressure is continuously varied. With adjustment of pressure, $CrGeTe_3$ alters from an insulator with $T_C \sim 66$ K at ambient pressure to a FM metal with T_C surpassing 250 K. The moderate decrease of T_C to ~54 K as pressure is raised to 4.5 GPa and subsequent dramatic fourfold rise of T_C in a rather narrow pressure range $4.5 \leq P \leq 6.5$ GPa emphasizes the competition between the FM insulating and FM metallic phase. The phase diagram also unearths a correlated 2D Fermi metal for $P \geq 7.0$ GPa, significantly well below the 2D to 3D structural transition (~18 GPa) [39], revealing a contrasting feature of $CrGeTe_3$ with $CrSiTe_3$ [38] and isostructural MPX_3 (M = V, Fe, Mn, Ni, and X = S, Se) compounds.

When pressurized, MPX_3 undergo an IMT accompanied by an isosymmetric structural transition, forming a M-M dimer due to direct overlap between neighboring t_{2g} orbitals of M ions [56–60]. Therefore, a spin crossover from high-spin to low-spin state occurs together with a large volume collapse. On the other hand, the nonexistence of such lattice change close to IMT of $CrGeTe_3$ [35,39] asserts that direct interaction between t_{2g} electrons of neighboring Cr atoms is still weak. In fact, this is compatible with the nearly pressure independence of M_S affirming the survival of the localized high spin ($S = 3/2$) state of t_{2g} manifolds even in a high pressure state [Fig. 4(b)]. Rather, these observations hint that the active Cr e_g orbital plays a major role in stabilizing the high pressure metallic state in $CrGeTe_3$, thus averting a structural transition as recently proposed for $NiPS_3$ [60]. Moreover, the remarkable absence of concomitant structural distortion across the IMT signifies that the pressure-induced modification of magnetic and electronic ground states of $CrGeTe_3$ is purely electronic in origin.

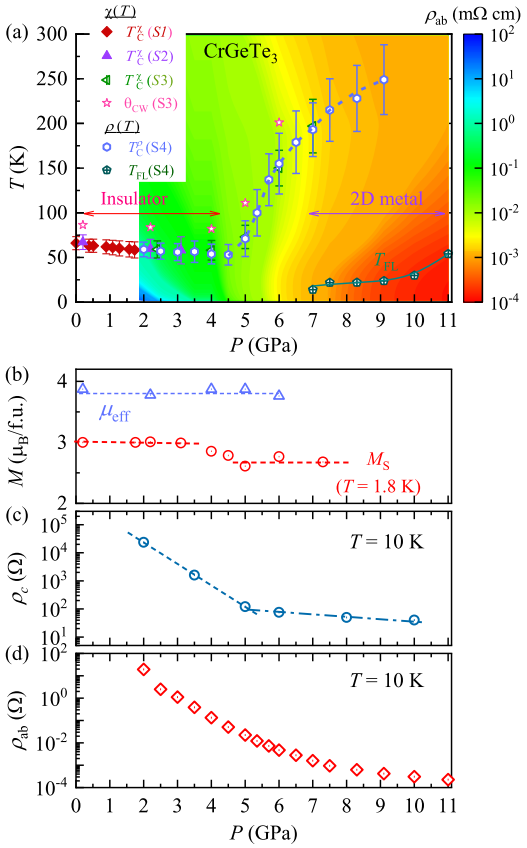

FIG. 4. (a) Pressure-temperature phase diagram of $CrGeTe_3$. Color scale represents the magnitude of ρ_{ab}. θ_{CW} and T_C^χ are estimated from magnetic susceptibility. T_C^ρ and T_{FL} are determined from ρ_{ab}. (b) Pressure dependence of effective moment, μ_{eff}, and saturation magnetic moment M_S (at $T = 1.8$ K). (c) and (d) are pressure dependence of ρ_c and ρ_{ab} at $T = 10$ K, respectively.

Now, we qualitatively explain the origin of such intriguing pressure dependent T_C of $CrGeTe_3$. In the 2D limit, the MAE, K, along with spin-exchange interaction J determine $T_C \sim J/\ln(3\pi J/4K)$ [61]. For $CrGeTe_3$, K ($\simeq -0.05$ meV), usually set by SOC and influencing the direction of magnetic easy axis [9,25], is much smaller in energy scale compared with J ($\simeq$3.0 meV) [9,62,63]. Thus, the strength of the exchange interaction plays a major role in fixing the T_C. As explained earlier in Fig. 1(c), the FM order in $CrGeTe_3$ is mainly driven by indirect superexchange interaction, J_{SE}, between Cr-e_g orbitals via two orthogonal Te-p orbitals. With such an orbital arrangement, the superexchange integral can be written as [64,65]

$$J_{SE} \sim -\frac{t_{pd}^2 t_{p'd'}^2 J_H^{Te}}{\Delta_{CT}^2 (2\Delta_{CT} + U_p)^2}, \quad (1)$$

where $t_{pd}(t_{p'd'})$ is the virtual hopping between the $e_g(e_g')$ and $p(p')$ orbital, J_H^{Te} is the Hund's coupling on the Te ion, U_p is the Coulomb interaction on the Te site, and Δ_{CT} is the

charge transfer energy gap between the Te p-valence band top and the bottom of the Cr e_g-conduction band. Also, J_{SE} depends on the geometrical Cr—Te—Cr bond angle θ. Pressure dependent x-ray diffraction studies reveal that θ deviates marginally from 90° under pressure even up to 10.0 GPa [35,39,62] and with such small deviation the J_{SE} exchange path remains robust [66]. Assuming J_H^{Te} to be unchanged with pressure, from Eq. (1) it is evident that a decrease of Δ_{CT} will have a much stronger impact on J_{SE} compared with others, since Δ_{CT} can be several times larger than t_{pd} and U_p. It is credible to expect Δ_{CT} tends to zero on approaching IMT with varying pressure. Indeed, a recent first principle calculation predicts the collapse of the p-d energy gap around 7.0 GPa as a result of a shortened Cr—Te bond [62]. Therefore, the sharp rise of T_C for $P \geq 4.5$ GPa can be attributed to the dramatic upsurge of intralayer J_{SE} resulting from the depreciation of Δ_{CT} with pressure. Here, it should be noted that Eq. (1) will become invalid after the gap Δ_{CT} is closed near the IMT. Closure of this gap is likely to open an indirect FM exchange pathway between localized t_{2g} electrons via itinerant carriers in bands touching the Fermi level and will dominate the total FM interaction over the J_{SE} path in metallic state.

The initial decrease of T_C and χ up to 4.5 GPa could be attributed to following reasons. Firstly, magnetostriction could be a possible reason for decreasing T_C [67], because Raman spectroscopy [35,69] and neutron diffraction [10] have detected evidence of strong magnetoelastic coupling across the FM transition of $CrGeTe_3$. Secondly, at ambient condition there exist finite AFM exchange interactions between the next nearest neighbor Cr atoms in the layer as well as between Cr atoms in adjacent layers [9,24,62,63], which can also contribute to the reduction of T_C. With growing pressure these AFM interactions will compete with J_{SE}, since they are expected to strengthen due to the shrinking distance between Cr atoms and vdW gaps between adjacent layers. Lastly, the sign change of K from negative to positive with pressure can trigger an alteration of magnetic easy axis from the c axis to the ab plane as reported in a pressure dependent magnetoresistance study [36]. However, when pressure exceeds 4.5 GPa, J_{SE} overcomes this competition due to a depreciating charge gap. The distinct pressure dependence of ρ_c and ρ_{ab} [as in Fig. 4(c) and 4(d)], back up the dominance of intralayer exchange interactions at the high pressure region. Up to 5.0 GPa, ρ_c drops more than 2 orders of magnitude, whereas it decreases barely in between 6.0 and 10.0 GPa. By contrast, ρ_{ab} continue to plunge up to 11.0 GPa. As well, the large $\rho_c/\rho_{ab} \sim 10^5$ in metallic state points out that carriers can hop more easily inside the layer rather than across the layers, making intralayer interactions significantly stronger than interlayer interactions.

In summary, we demonstrate that pressure can be used as a suitable parameter to control both magnetic and electrical properties of $CrGeTe_3$ by tuning the charge transfer energy gap between the Te-p valence band and Cr-e_g conduction band. Moreover, lack of concurrent structural transition and spin crossover across the IMT makes $CrGeTe_3$ a unique vdW material and provides a novel example of bandwidth-controlled IMT.

We acknowledge fruitful discussions with J.-G. Cheng, K. Matsubayashi, M. K. Ray and K. Murata. This work was financially supported by the JSPS KAKENHI Grants No. JP19H00648 and No. 19H01836. The work at SNU was supported by Grants No. 2019R1A2C2090648, No. 2019M3E4A1080227, and No. 2016K1A4A3914691 through the National Research Foundation of Korea funded by the Korean government.

*dilipkbhoi@issp.u-tokyo.ac.jp

[1] K. S. Burch, D. Mandrus, and J.-G. Park, Nature (London) **563**, 47 (2018).
[2] B. Huang, M. A. McGuire, A. F. May, D. Xiao, P. Jarillo-Herrero, and X. Xu, Nat. Mater. **19**, 1276 (2020).
[3] C. Gong and X. Zhang, Science **363**, eaav4450 (2019).
[4] D. Zhong, K. L. Seyler, X. Linpeng, R. Cheng, N. Sivadas, B. Huang, E. Schmidgall, T. Taniguchi, K. Watanabe, M. A. McGuire *et al.*, Sci. Adv. **3**, e1603113 (2017).
[5] X. Yao, B. Gao, M.-G. Han, D. Jain, J. Moon, J. W. Kim, Y. Zhu, S.-W. Cheong, and S. Oh, Nano Lett. **19**, 4567 (2019).
[6] K. L. Seyler, D. Zhong, B. Huang, X. Linpeng, N. P. Wilson, T. Taniguchi, K. Watanabe, W. Yao, D. Xiao, M. A. McGuire, Kai-Mei C. Fu, and X. Xu, Nano Lett. **18**, 3823 (2018).
[7] C. Xu, J. Feng, M. Kawamura, Y. Yamaji, Y. Nahas, S. Prokhorenko, Y. Qi, H. Xiang, and L. Bellaiche, Phys. Rev. Lett. **124**, 087205 (2020).
[8] C. Xu, J. Feng, H. Xiang, and L. Bellaiche, npj Comput. Mater. **4**, 57 (2018).
[9] C. Gong, L. Li, Z. Li, H. Ji, A. Stern, Y. Xia, T. Cao, W. Bao, C. Wang, Y. Wang *et al.*, Nature (London) **546**, 265 (2017).
[10] V. Carteaux, D. Brunet, G. Ouvrard, and G. Andre *et al.*, J. Phys. Condens. Matter **7**, 69 (1995).
[11] M. A. McGuire, H. Dixit, V. R. Cooper, and B. C. Sales, Chem. Mater. **27**, 612 (2015).
[12] I. Tsubokawa, J. Phys. Soc. Jpn. **15**, 1664 (1960).
[13] B. Huang, G. Clark, E. Navarro-Moratalla, D. R. Klein, R. Cheng, K. L. Seyler, D. Zhong, E. Schmidgall, M. A. McGuire *et al.*, Nature (London) **546**, 270 (2017).
[14] Z. Zhang, J. Shang, C. Jiang, A. Rasmita, W. Gao, and T. Yu, Nano Lett. **19**, 3138 (2019).
[15] H. H. Kim, B. Yang, S. Li, S. Jiang, C. Jin, Z. Tao, G. Nichols, F. Sfigakis, S. Zhong, C. Li, S. Tian *et al.*, Proc. Natl. Acad. Sci. U.S.A. **116**, 11131 (2019).
[16] D. C. Freitas, R. Weht, A. Sulpice, G. Remenyi, P. Strobel, F. Gay, J. Marcus, and M. N.-Regueiro, J. Phys. Condens. Matter **27**, 176002 (2015).
[17] X. Zhang, Q. Lu, W. Liu, W. Niu, J. Sun, J. Cook, M. Vaninger, P. F. Miceli, D. J. Singh, S.-W. Lian *et al.*, Nat. Commun. **12**, 2492 (2021).
[18] H. J. Deiseroth, K. Aleksandrov, C. Reiner, L. Kienle, and R. K. Kremer, Eur. J. Inorg. Chem. **2006**, 1561 (2006).

[19] B. Chen, J. Yang, H. D. Wang, M. Imai, H. Ohta, C. Michioka, K. Yoshimura, and M. Fang, J. Phys. Soc. Jpn. **82**, 124711 (2013).

[20] Y. Deng, Y. Yu, Y. Song, J. Zhang, N. Z. Wang, Z. Sun, Y. Yi, Y. Z. Wu, S. Wu, J. Zhu *et al.*, Nature (London) **563**, 94 (2018).

[21] Z. Fei, B. Huang, P. Malinowski, W. Wang, T. Song, J. Sanchez, W. Yao, Di Xiao, X. Zhu, A. F. May *et al.*, Nat. Mater. **17**, 778 (2018).

[22] S. Kang, S. Kang, and J. Yu, J. Electron. Mater. **48**, 1441 (2019).

[23] M. Suzuki, B. Gao, K. Koshiishi, S. Nakata, K. Hagiwara, C. Lin, Y. X. Wan, H. Kumigashira, K. Ono, S. Kang, S. Kang, J. Yu, M. Kobayashi, S. W. Cheong, and A. Fujimori, Phys. Rev. B **99**, 161401(R) (2019).

[24] J. Zhang, X. Cai, W. Xia, A. Liang, J. Huang, C. Wang, L. Yang, H. Yuan, Y. Chen, S. Zhang, Y. Guo, Z. Liu, and G. Li, Phys. Rev. Lett. **123**, 047203 (2019).

[25] D.-H. Kim, K. Kim, K.-T. Ko, J. H. Seo, J. S. Kim, T.-H. Jang, Y. Kim, J.-Y. Kim, S.-W. Cheong, and J.-H. Park, Phys. Rev. Lett. **122**, 207201 (2019).

[26] M. D. Watson, I. Marković, F. Mazzola, A. Rajan, E. A. Morales, D. M. Burn, T. Hesjedal, G. van der Laan, S. Mukherjee, T. K. Kim, C. Bigi, I. Vobornik, M. Ciomaga Hatnean, G. Balakrishnan, and P. D. C. King, Phys. Rev. B **101**, 205125 (2020).

[27] A. K. Kundu, Y. Liu, C. Petrovic, and T. Valla, Sci. Rep. **10**, 15602 (2020).

[28] Z. Wang, T. Zhang, M. Ding, B. Dong, Y. Li, M. Chen, X. Li, J. Huang, H. Wang, X. Zhao *et al.*, Nat. Nanotechnol. **13**, 554 (2018).

[29] S. Jiang, L. Li, Z. Wang, K. F. Mak, and J. Shan, Nat. Nanotechnol. **13**, 549 (2018).

[30] I. A. Verzhbitskiy, H. Kurebayashi, H. Cheng, J. Zhou, S. Khan, Y. P. Feng, and G. Eda, National electronics review **3**, 460 (2020).

[31] N. Wang, H. Tang, M. Shi, H. Zhang, W. Zhuo, D. Liu, F. Meng, L. Ma, J. Ying, L. Zou *et al.*, J. Am. Chem. Soc. **141**, 17166 (2019).

[32] D. Weber, A. H. Trout, D. W. McComb, and J. E. Goldberge, Nano Lett. **19**, 5031 (2019).

[33] T. Song, Z. Fei, M. Yankowitz, Z. Lin, Q. Jiang, K. Hwangbo, Q. Zhang, B. Sun, T. Taniguchi, K. Watanabe *et al.*, Nat. Mater. **18**, 1298 (2019).

[34] T. Li, S. Jiang, N. Sivadas, Z. Wang, Y. Xu, D. Weber, J. E. Goldberger, K. Watanabe, T. Taniguchi, C. J. Fennie *et al.*, Nat. Mater. **18**, 1303 (2019).

[35] Y. Sun, R. C. Xiao, G. T. Lin, R. R. Zhang, L. S. Ling, Z. W. Ma, X. Luo, W. J. Lu, Y. P. Sun, and Z. G. Sheng, Appl. Phys. Lett. **112**, 072409 (2018).

[36] Z. Lin, M. Lohmann, Z. A. Ali, C. Tang, J. Li, W. Xing, J. Zhong, S. Jia, W. Han, S. Coh, W. Beyermann, and J. Shi, Phys. Rev. Mater. **2**, 051004(R) (2018).

[37] S. Mondal, M. Kannan, M. Das, L. Govindaraj, R. Singha, B. Satpati, S. Arumugam, and P. Mandal, Phys. Rev. B **99**, 180407(R) (2019).

[38] W. Cai, H. Sun, W. Xia, C. Wu, Y. Liu, H. Liu, Y. Gong, D.-X. Yao, Y. Guo, and M. Wang, Phys. Rev. B **102**, 144525 (2020).

[39] Z. Yu, W. Xia, K. Xu, M. Xu, H. Wang, X. Wang, N. Yu, Z. Zou, J. Zhao, L. Wang, X. Miao, and Y. Guo, J. Phys. Chem. C **123**, 13885 (2019).

[40] H. Ji, R. A. Stokes, L. D. Alegria, E. C. Blomberg, M. A. Tanatar, A. Reijnders, L. M. Schoop, T. Liang, R. Prozorov, K. S. Burch *et al.*, J. Appl. Phys. **114**, 114907 (2013).

[41] Y. Liu and C. Petrovic, Phys. Rev. B **96**, 054406 (2017).

[42] W. Liu, Y. Dai, Y.-E. Yang, J. Fan, L. Pi, L. Zhang, and Y. Zhang, Phys. Rev. B **98**, 214420 (2018).

[43] See Supplemental Material at http://link.aps.org/supplemental/10.1103/PhysRevLett.127.217203 for more details of single crystal growth and characterization, magnetization and resistivity measurements techniques under high pressure, which includes Refs. [35,40,44–51].

[44] N. Hiraoka, K. Whiteaker, M. Blankenhorn, Y. Hayashi, R. Oka, H. Takagi, and K. Kitagawa, J. Phys. Soc. Jpn. **90**, 074001 (2021).

[45] Y. Uwatoko, T. Fujiwara, M. Hedo, F. Tomioka, and I. Umehara, J. Phys. Condens. Matter **17**, S1011 (2005).

[46] K. Yokogawa, K. Murata, H. Yoshino, and S. Aoyama, Jpn. J. Appl. Phys. **46**, 3636 (2007).

[47] *MPMS Application Note* (Quantum Design, Inc., 2002), pp. 1014–1213.

[48] I. A. Eiling and J. S. Schilling, J. Phys. F **11**, 623 (1981).

[49] D. Staško, J. Prchal, M. Klicpera, S. Aoki, and K. Murata, High Press. Res. **40**, 525 (2020).

[50] J.-G. Cheng, K. Matsubayashi, S. Nagasaki, A. Hisada, T. Hirayama, M. Hedo, H. Kagi, and Y. Uwatoko, Rev. Sci. Instrum. **85**, 093907 (2014).

[51] N. Mori, H. Takahashi, and N. Takeshita, High Press. Res. **24**, 225 (2004).

[52] O. Gunnarsson, M. Calandra, and J. E. Han, Rev. Mod. Phys. **75**, 1085 (2003).

[53] S. Ono and Y. Ando, J. Phys. C **388–389**, 321 (2003).

[54] H. Kuwahara, T. Okuda, Y. Tomioka, A. Asamitsu, and Y. Tokura, Phys. Rev. Lett. **82**, 4316 (1999).

[55] Y. Shimizu and R. Kato, Phys. Rev. B **97**, 125107 (2018).

[56] Y. Wang, Z. Zhou, T. Wen, Y. Zhou, N. Li, F. Han, Y. Xiao, P. Chow, J. Sun, M. Pravica *et al.*, J. Am. Chem. Soc. **138**, 15751 (2016).

[57] C. R. S. Haines, M. J. Coak, A. R. Wildes, G. I. Lampronti, C. Liu, P. Nahai-Williamson, H. Hamidov, D. Daisenberger, and S. S. Saxena, Phys. Rev. Lett. **121**, 266801 (2018).

[58] Y. Wang, J. Ying, Z. Zhou, J. Sun, T. Wen, Y. Zhou, N. Li, Q. Zhang, F. Han, Y. Xiao *et al.*, Nat. Commun. **9**, 1914 (2018).

[59] M. J. Coak, S. Son, D. Daisenberger, H. Hamidov, C. R. S. Haines, P. L. Alireza, A. R. Wildes, C. Liu, S. S. Saxena, and Je-Geun Park, npj Quantum Mater. **4**, 38 (2019).

[60] H. S. Kim, K. Haule, and D. Vanderbilt, Phys. Rev. Lett. **123**, 236401 (2019).

[61] Myron Bander and D. L. Mills, Phys. Rev. B **38**, 12015(R) (1988).

[62] A. O. Fumega, S. Blanco-Canosa, H. Babu-Vasili, P. Gargiani, H. Li, J.-S. Zhou, F. Rivadulla, and V. Pardo, J. Mater. Chem. C **8**, 13582 (2020).

[63] G. Menichetti, M. Calandra, and M. Polini, 2D Mater. **6**, 045042 (2019).

[64] S. V. Streltsov and D. I. Khomskii, Phys. Rev. B **77**, 064405 (2008).

[65] D. I. Khomskii, K. I. Kugel, A. O. Sboychakov, and S. V. Streltsov, J. Exp. Theor. Phys. **122**, 484 (2016).
[66] X. J. Dong, J. Y. You, Z. Zhang, B. Gu, and G. Su, Phys. Rev. B **102**, 144443 (2020).
[67] For a second order phase transition, the shift of T_C with hydrostatic pressure can be deduced using the Ehrenfest equation [68]: $dT_C/dP = T_C V \Delta\alpha_V/\Delta C$, where $\Delta\alpha_V = \Delta[(dV/dT)/T]V$ and ΔC are the jump of volume thermal expansion coefficient and heat capacity at T_C. A negative $\Delta\alpha_V$ can be anticipated from the temperature dependence of unit cell parameters of $CrGeTe_3$ [10], consequently making dT_C/dP negative.
[68] P. Ehrenfest, Proc. R. Acad. Amsterdam **36**, 153 (1933).
[69] Y. Tian, M. J. Gray, H. Ji, R. J. Cava, and K. S. Burch, 2D Mater. **3**, 025035 (2016).